μSR study of short-range magnetic order in the paramagnetic regime of $ErCo_2$

C. M. Bonilla*
Instituto de Ciencia de Materiales de Aragón and Departamento de Física de la Materia Condensada, CSIC - Universidad de Zaragoza, Pedro Cerbuna 12, E-50009 Zaragoza, Spain

N. Marcano
Centro Universitario de la Defensa, Ctra. de Huesca s/n, E-50090 Zaragoza, Spain and
Instituto de Ciencia de Materiales de Aragón and CSIC - Universidad de Zaragoza, Departamento de Física de la Materia Condensada, Pedro Cerbuna 12, E-50009 Zaragoza, Spain

J. Herrero-Albillos
Helmholtz-Zentrum Berlin für Materialien und Energie GmbH, Albert-Einstein-Straße 15, D-12489 Berlin, Germany,
Centro Universitario de la Defensa, Carretera de Huesca s/n, E-50090 Zaragoza, Spain, and
Instituto de Ciencia de Materiales de Aragón and Departamento de Física de la Materia Condensada, CSIC - Universidad de Zaragoza, Pedro Cerbuna 12, E-50009 Zaragoza, Spain

A. Maisuradze
Laboratory for Muon Spin Spectroscopy, Paul Scherrer Institute, CH-5232 Villigen PSI, Switzerland and
Physik-Institut der Universität Zürich, Winterhurestrasse 190, CH-8057 Zürich, Switzerland

L. M. García and F. Bartolomé
Instituto de Ciencia de Materiales de Aragón and Dpto. de Física de la Materia Condensada, CSIC - Universidad de Zaragoza, Pedro Cerbuna 12, E-50009 Zaragoza, Spain

(Received 26 May 2011; revised manuscript received 27 September 2011; published 16 November 2011)

Zero-field muon spin relaxation spectroscopy (μSR) measurements in the paramagnetic phase of $ErCo_2$ ferrimagnetic system are reported. Previous experimental studies using macro- and microscopic techniques led to the identification of magnetic short-range correlations between the Co atoms in the paramagnetic state of this material. The analysis of μSR spectra recorded on $ErCo_2$ well above T_c indicates two dynamical magnetic processes characterized by remarkably different relaxation rates: a slow-relaxing signal, which quantitatively coincides with previous μSR studies on $ErAl_2$, and fast-relaxing signal, which can be ascribed to the Co short-range correlated regions observed above T_c. Moreover, the μSR technique provides information on the thermal dependence of Co correlated regions at true zero field. These findings shed light on the dynamical nature of the clustered phase developing in the paramagnetic state of $ErCo_2$.

DOI: 10.1103/PhysRevB.84.184425 PACS number(s): 75.50.Gg, 71.20.Lp, 81.30.Bx, 76.75.+i

I. INTRODUCTION

The scientific interest in cobalt-rich rare-earth (R) intermetallic compounds such as the Co Laves phases, RCo_2, has been active since the 1960s due to the wide range of magnetic properties of these compounds such as itinerant-electron metamagnetism, high transition temperatures, large saturation magnetization, and the potential technological applications of these materials in the design of magnetocaloric devices.[1–4] In particular, the study of the Co band has been the subject of intense investigation for decades.[5–13] In these compounds, the Co sublattice is near the critical condition for the formation of magnetic moment, turning the Co 3d-electron system very sensitive to the internal field created by the R sublattice or to changes of external parameters. Particularly unique is the case of the Co sublattice in $ErCo_2$, as it is just above the condition for undergoing a metamagnetic transition.[1,7,14,15]

The $ErCo_2$ structure is cubic above the first-order ferrimagnetic ordering transition ($T_c = 32$ K at $H = 0$ T), which has an associated rhombohedral distortion of the crystal structure.[16] The magnetic behavior of the compound is mostly dominated by the Er sublattice at all temperatures. The magnetic moment of the Er^{3+} ions is essentially temperature independent and has been determined by neutron diffraction and magnetic susceptibility as $m_{Er} = 8.8\,\mu_B$,[17] much larger than the magnetic moment of the two Co atoms per formula unit. Hence, when a magnetic field is applied, the Er net magnetic moment is parallel to the applied field. Below T_c, the Co 3d moments order antiparallel to the applied magnetic field, with a magnetic moment of around 0.9 μ_B per Co atom.[17] However, the behavior of the Co sublattice above T_c is rather more complex and, indeed, recent studies in the $ErCo_2$ paramagnetic phase have revealed new and interesting phenomena related to the Co 3d moment. On the one hand, the existence of an intrinsic (although small) Co moment well above the ordering transition was recently demonstrated,[18] solving an enduring controversy on its existence.[19–21] On the other hand, the presence of sizable magnetic short-range correlated regions in the paramagnetic phase of $ErCo_2$ has been observed by small-angle neutron scattering (SANS), with magnetic clusters of about 8 Å in size present at 60 K.[22] An anomaly in the ac magnetic susceptibility $\chi_{ac}(T)$ curves at zero field in the paramagnetic regime has been attributed as due to the contribution from the magnetic clusters.

The magnitude of the observed anomaly in ac susceptibility and the size of the magnetic clusters as determined by SANS measurements are indicative of clusters formed by Co only with a magnetic moment of about $m_{Co} = 0.2\ \mu_B$. The formation of these Co clusters corroborates that Co-Co is by far the strongest magnetic interaction present in the system.[23–25]

X-ray circular magnetic dichroism (XMCD) measurements were performed at the Er $M_{4,5}$ and Co $L_{2,3}$ absorption edges, from below to well above the ferrimagnetic ordering temperature (5 K $< T <$ 100 K). The measurements at the Er $M_{4,5}$ edges confirmed that the Er $4f$ magnetic moment, being the largest one in the system, remains parallel to the applied field (H_{app}) both above and below the ordering temperature. However, temperature-dependent XMCD at the Co $L_{2,3}$ edges shows that the Co $3d$ magnetization changes sign not at the ferrimagnetic transition temperature, but at a certain temperature coined as the flipping temperature (T_f), considerably higher than T_c. Indeed, at $H = 1$ T the flipping temperature $T_f \approx 2T_c$, while for lower applied fields T_f reaches $3T_c$. This new magnetic configuration in $ErCo_2$ (denoted *parimagnetism*)[22] and the formation of magnetic clusters of Co moments has recently been identified with the stabilization of a Griffiths-like phase in paramagnetic $ErCo_2$.[26]

In the region $T_c < T < T_f$, the antiferromagnetic (AF) coupling with Er is minimized by the creation of Co clusters, which also satisfies the stronger Co-Co ferromagnetic interaction, as this reduces the average number of antiparallel alignments between Co nearest neighbors. Therefore, the occurrence of Co magnetic clusters gives rise to the negative Co magnetization (i.e., antiparallel to H_{app}) at a temperature considerably higher than T_c. Additionally, within the paramagnetic phase of $ErCo_2$ there is a narrow temperature range around T_f at which the net sign of the Co moments are still determined by the AF exchange with Er, but the effect of the applied magnetic field on the orbital Co moment overcomes the action of the spin orbit interaction, giving rise to a pseudoviolation of the third Hund's rule.[27]

As a result of combined analysis of SANS, XMCD, and ac susceptibility χ_{ac} experiments, three regions can be identified in the magnetic phase diagram of $ErCo_2$, as shown in Fig. 1. The paramagnetic region at temperatures above the first-order magnetic transition (□) is divided into two regions: the parimagnetic one at $T_c < T < T_f$ and the usual paramagnetic one at $T > T_c$. These two magnetic configurations are separated by the flipping temperature curve (◇) determined for different values of applied magnetic field.

It is worth mentioning that the temperature at which the Co magnetic clusters are formed in $ErCo_2$, as well as their spin dynamics, is still an open question. Indeed, a complete description of the dynamic character of magnetic clustered systems requires the use of a wide variety of experimental techniques in order to obtain information at various time scales. While χ_{ac} measured with a standard magnetometer is able to detect spin dynamic rates between 10^{-2} Hz and 10^3 Hz, neutron scattering is sensitive to rates from 10^9 Hz to 10^{14} Hz. Muon spin relaxation spectroscopy (μSR) allows exploring the intermediate time window, from 10^4 Hz up to 10^{12} Hz (see Ref. 28), making this technique well suited for studying static or quasistatic spin correlations.

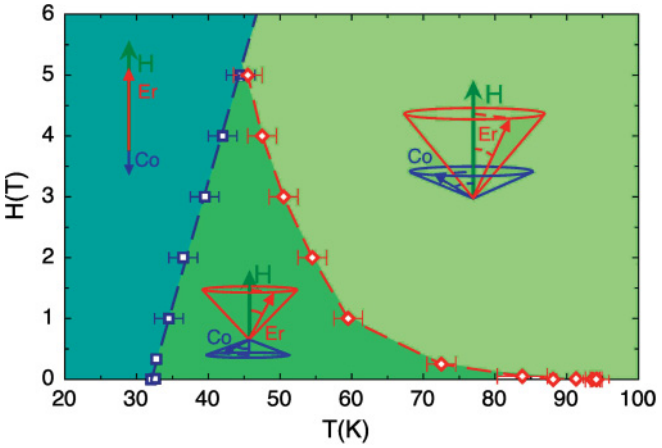

FIG. 1. (Color online) Magnetic phase diagram of $ErCo_2$. Squares (□) indicate the critical temperature obtained from macroscopic magnetization measurements and XMCD. Diamonds (◇) indicate the flipping temperature T_f obtained from XMCD, SANS, and paramagnetic susceptibility measurements (Ref. 22).

Moreover, muon is a local probe which provides information on the magnetic coupling between the magnetic ions surrounding it, at true zero field. The fact that muon is a microscopic probe of the magnetism on the sample which needs no large coherence length is relevant for the aim of the present study since it is very sensitive to short-range and other forms of disordered magnetism (cluster-glass, spin-glass).[29,30] A detailed description of muon spin relaxation spectroscopy can be found in Refs. 28, 31, 32, and 33.

The muon sensitivity to short-range order and other forms of disordered magnetism (cluster-glass, spin-glass) has been used to study the magnetic inhomogeneities at low temperature in systems such as $CeCu_2Si_2$,[30], $FeCr_2S_4$,[34] $CeNi_{1-x}Cu_x$,[29] RMn_4Al_8,[35] spinels $(Mn,Fe,Co)Al_2O_4$,[36] and the ferromagnetic manganite $La_{1-x}Ca_xMnO_3$,[37] among others. In these examples, the different spin dynamics (namely multiple spin fluctuation rates) detected by the analysis of the μSR spectra are a signature of heterogeneous magnetic phases, including ordered clusters within the paramagnetic regime.[29] In the same way, our results on μSR spectroscopy give insight on the nature of the unusual paramagnetic state of $ErCo_2$.

II. EXPERIMENTAL DETAILS

Polycrystalline samples of $ErCo_2$ were prepared in an arc furnace under Ar atmosphere, by melting together stoichiometric amounts of metallic precursors. The annealing was done under Ar atmosphere at 850 °C for one week in order to improve the homogeneity. X-ray diffraction analysis on powdered samples was performed in a Rigaku RTO 500RC diffractometer with Bragg-Brentano geometry and using Kα-Cu radiation at room temperature. Neutron diffraction measurements at low temperatures were performed at the D2B high-resolution diffractometer at Institut Laue Langevin. The x-ray and neutron diffractograms together with their Rietveld refinements can be found in Refs. 4 and 22, respectively. The samples were also analyzed by scanning electron microscopy and energy dispersive spectroscopy (EDS) showing a highly pure phase within the limits of detection of each technique.

The magnetic characterization was performed under applied magnetic fields up to 9 T at the Servicio de Medidas Físicas of the University of Zaragoza-CSIC. A comprehensive study of the thermodynamic and magnetic properties of the very same samples used in this study has been published in Refs. 4, 22, and 26.

μSR measurements in zero field (ZF) and transverse field (TF) were carried out at the πM3 surface muon beam line at the Swiss muon source (SμS) in the Paul Scherrer Institute (Switzerland) using the General Purpose Spectrometer (GPS). This spectrometer offers a He-flow cryostat for temperatures ranging from 1.5 K up to 300 K. The detection system contains a so-called *veto* circuit for the suppression of the μSR signal arising from muons stopped outside the sample (i.e., background signal). The spectrometer dead time is 5 ns. Small ingots of the sample were mounted between aluminized mylar foils, the recommended mounting procedure in connection with the veto circuit. The muon spin relaxation measurements on the $ErCo_2$ sample were performed between $28\ \text{K} \leqslant T \leqslant 300\ \text{K}$.

In a μSR experiment, a beam of nearly a 100% spin polarized positive (anti)muons is directed toward the sample. Each muon is implanted in the sample and comes to rest (usually at an interstitial lattice position) and later decay into a positron with a mean life of 2.2 μs. The positron is then emitted preferably in the direction of the muon spin axis. These positrons are detected and time stamped in the detectors which are positioned before (F) and after (B) the sample. Assuming that both detectors work the same way, the histogram of a large number of counts allows one to obtain "raw asymmetry" as function of time:

$$A_{\text{raw}}(t) = \frac{N_F(t) - N_B(t)}{N_F(t) + N_B(t)}, \tag{1}$$

where $N_F(t)$, $N_B(t)$ are the positron count rates for each detector.

In order to take into account the relative counting efficiency of the two detectors [$\alpha = N_B(0)/N_F(0)$] a corrected asymmetry [$A(t)$] is determined as follows:

$$A(t) = \frac{(\alpha - 1) + (\alpha + 1)A_{\text{raw}}}{(\alpha + 1) + (\alpha - 1)A_{\text{raw}}}. \tag{2}$$

The value of α is experimentally determined from the fit of a known spectral response. To do so, an external field is applied perpendicular to the beam direction (this is the so-called TF measurement) giving rise to an oscillatory pattern, whose typical muon response function allows the determination of α. By substituting Eq. (1) into Eq. (2) the asymmetry can be also written as

$$A(t) = \frac{\alpha N_F(t) - N_B(t)}{\alpha N_F(t) + N_B(t)}, \tag{3}$$

which is a standard expression for a convenient visualization of the data.[31] However for technical reasons, during the fitting process, it is more useful to keep the data constant (parameter independent) while changing the parameter α. For that reason, one fits the raw data as represented by Eq. (1).

We recorded spectra in the TF setup at selected temperatures (28 K, 50 K, 100 K, and 200 K) and a 3 mT transverse field has been applied. The zero-field spectra were collected heating the sample to room temperature in zero field.

III. RESULTS AND DISCUSSION

The ZF-μSR signal from a magnetically ordered and paramagnetic samples is described by different response functions.[28] Therefore, we will present our analysis of the spectra recorded below and above T_c in two independent subsections.

A. Long-range-order regime

The $ErCo_2$ ZF-μSR spectra measured in the ferrimagnetic phase show the typical response for an ordered magnet. The isothermal measurements were taken in the ferrimagnetic state at 20 K, 24 K, and 28 K. Figure 2 shows the ZF spectrum measured at 24 K as representative of this study. As expected, a damped oscillatory signal can be observed below T_c. The periodic arrangement of the magnetic moments in a long-range-ordered (LRO) system creates a nonzero mean field $\langle B_\mu \rangle$ at the muon stopping site. Therefore the muon spin precesses due to the component of the field perpendicular to the initial muon spin polarization leading to an oscillatory response of the asymmetry versus time. For a magnetically ordered polycrystalline sample, the ZF-μSR spectrum from a magnetically ordered polycrystalline sample can be described by

$$A(t) = A_0\left[\tfrac{2}{3}\exp(-\lambda_{\text{tr}}t)\cos(\gamma_\mu\langle B_\mu\rangle t + \phi) + \tfrac{1}{3}\exp(-\lambda_{\text{lg}}t)\right], \tag{4}$$

where A_0 is the initial asymmetry (at $t = 0$) denoting the signal strength and $\langle B_\mu \rangle$ reflects the thermal average of the effective moment at the muon site. The oscillatory term due to the coherent precession of the muon spins with a component of their spin polarization perpendicular to the local field $\langle B_\mu \rangle$ is described by the cosine factor where γ_μ is the gyromagnetic

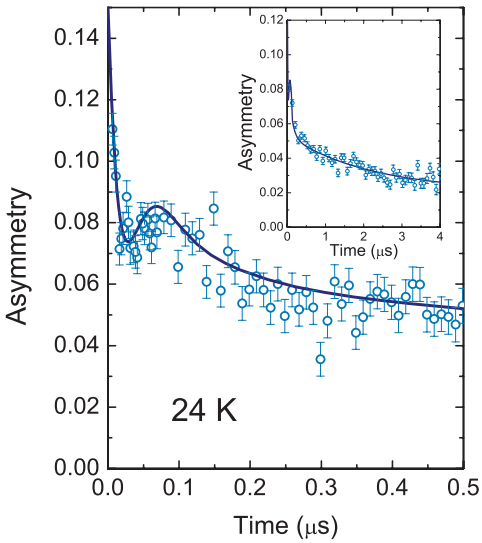

FIG. 2. (Color online) ZF-μSR spectrum recorded at 24 K in the ferrimagnetic phase. Solid line is the least-squares fit to Eq. (4). The inset shows the extended time scale up to 4 μs.

TABLE I. Fitting parameters for ZF-μSR spectra recorded on $ErCo_2$ for $T < T_c$.

Temperature (K)	A_0	λ_{tr} (μs^{-1})	$\langle B_\mu \rangle$ (mT)	λ_{lg} (μs^{-1})
20	0.17	50(5)	50(5)	10(1.5)
24	0.17	43(4)	47(5)	12(1)
28	0.17	60(9)	32(5)	18(1)

ratio for the muon (≈851 MHz/T) and ϕ is a phase shift, (in this case $\phi = 0$). Local imperfections in the long-range-order spin arrangement gives rise to a static distribution of the local field around its mean value $\langle B_\mu \rangle$, which leads to a damping of the oscillatory pattern described by the exponential term containing the transverse relaxation rate λ_{tr}. The term multiplied by 1/3 accounts for those components of the muon spin that are expected to lie parallel to $\langle B_\mu \rangle$. It consists on an exponential loss of initial muon spin polarization with the characteristic relaxation rate λ_{lg}.

All spectral responses recorded below T_c can be described by Eq. (4). The parameters resulting from the fit are given in Table I. It is worth mentioning that the experimental signal is strongly damped in $ErCo_2$, and only a few oscillations can be seen. A fast damping of the oscillatory signal evidences a rather broad static distribution of $\langle B_\mu \rangle$. Previous results in ordered Er compounds by Öner *et al*. reveal the complexity of the magnetic state of this system even in the ordered regime,[25,38,39] in agreement with the broad distribution of local field observed below T_c in the μSR spectra for the $ErCo_2$.

B. Paramagnetic regime

Figure 3 shows the ZF-μSR spectra at representative temperatures above T_c. In the paramagnetic regime the thermally induced magnetic disorder implies a randomly oriented spin ensemble, both in time and space, so $\langle B_\mu \rangle = 0$ avoiding the muon spin precession to take place. As result, the oscillatory term in Eq. (4) vanishes. Thus, for a powder polycrystalline sample the μSR spectrum can be fitted to an exponential relaxation function[28,40]

$$A(t) = A_0 \exp(-\lambda_{par} t), \tag{5}$$

where A_0 denotes the initial asymmetry, $\lambda_{par} = \gamma_\mu^2 \langle B_\mu^2 \rangle \tau$ is the relaxation rate, and the fluctuation rate of the magnetic moments surrounding the muon is given by $1/\tau$.

The data measured at the temperature range 127 K < T < 300 K have been successfully fitted to the muon spin relaxation function described in Eq. (5). A usual value for the relaxation rate in the fast-fluctuation limit, $\lambda_{par} = 0.56 \mu s^{-1}$, has been obtained in the spectrum measured at 300 K. However, the shape of the exponential decay of the data changes dramatically as the temperature decreases, as can be observed in Fig. 3. A comparison between two paramagnetic ZF-μSR spectra, recorded at temperatures above and below 127 K (300 K and 60 K, respectively) is shown in Fig. 4. Whereas a single exponential is enough to describe the 300 K spectrum, the situation is clearly different at 60 K, as the shape of this spectrum shows an initial fast decay and then a much slower one. The data cannot be fitted by a single exponential. The best fitting for ZF-μSR spectra at temperatures below

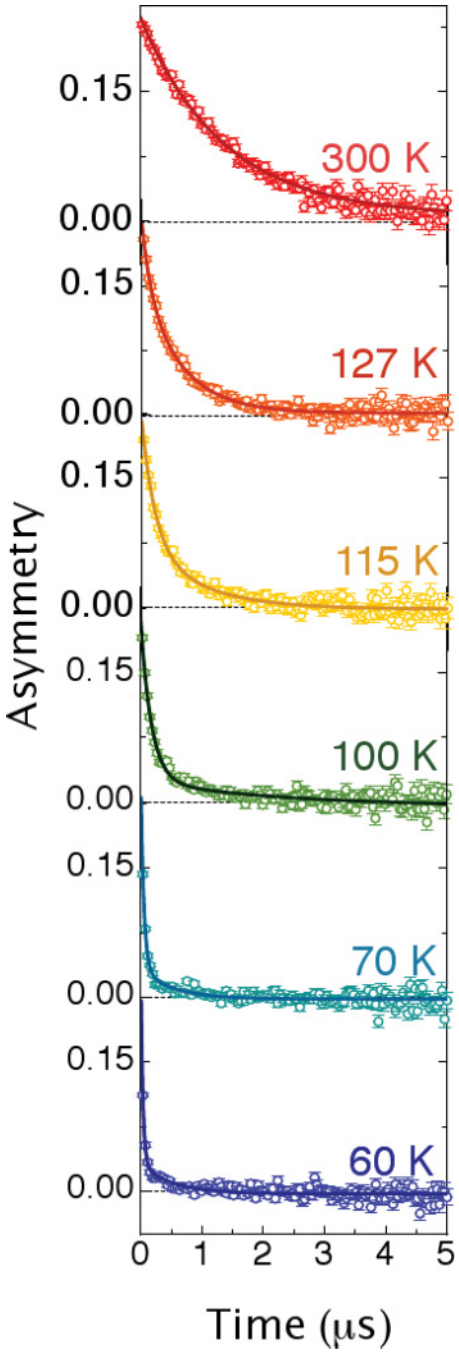

FIG. 3. (Color online) Typical examples of ZF-μSR spectra of $ErCo_2$ measured at temperatures above T_c. Data obtained in GPS facility (open symbols). Solid lines are the least-squares fits to Eq. (5) or (6) (see text).

127 K and above T_c is achieved with a two-exponential function where the sum of two paramagnetic responses with two different relaxation rates is used:

$$A(t) = A_{fast} \exp(-\lambda_{fast} t) + A_{slow} \exp(-\lambda_{slow} t). \tag{6}$$

In the thick continuous line we can observe that a satisfactory fit to Eq. (6) can be achieved with the sum of two paramagnetic decays. The slow and fast decay exponential functions are represented by the dotted and solid lines, respectively. The two-exponential function describes the ZF-μSR spectra in a wide

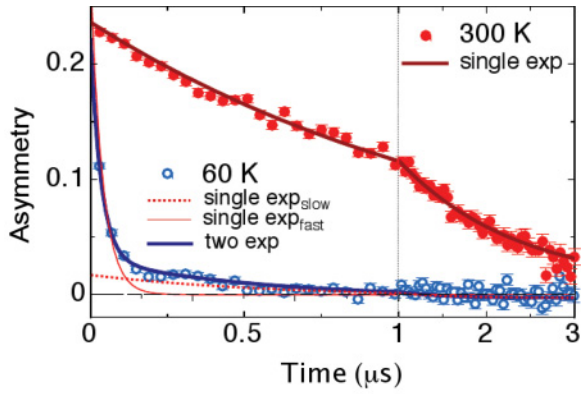

FIG. 4. (Color online) Comparison between two ZF-μSR spectra measured in the paramagnetic phase. Shown are the data recorded at 300 K and 60 K (full and open symbols) and their least-squares fit to Eqs. (5) and (6), respectively (thick solid lines). Thin dotted and solid lines are two exponential functions, with a slow decaying rate and a fast decaying rate, respectively. The sum of these two single exponential functions corresponds to the least-squares fit for data at 60 K.

temperature range ($T_c < T < 127$ K) within the paramagnetic regime. It is worth mentioning that for temperatures below 50 K and above T_c the rapid initial decay of asymmetry leads to the loss of most of the fast signal in the instrument dead time. The initial asymmetry must remain constant independently of the temperature when measuring under the same geometric conditions. Hence, in order to avoid an artifactual conclusion from our data we fix $A_0 = A_{fast} + A_{slow}$, in the whole temperature range below 127 K.

TF spectra support the two-relaxing-signal scenario within the paramagnetic regime for $T_c < T < 127$ K. TF data have been used before to obtain the initial asymmetry A_0 value in the case of a sample signal consisting of several components.[41] Figure 5 shows the TF spectra collected at 200 K and 50 K with a transverse field of 3 mT. As result of the muon spin precession the TF measurements lead to an oscillatory pattern:

$$A(t) = A_0 \exp[-\lambda t] \cos(\gamma_\mu \langle B_\mu \rangle t + \phi). \quad (7)$$

TF spectrum at 200 K can be fitted with the single oscillatory signal, described in Eq. (7). By contrast, the TF spectrum at 50 K requires two oscillating signals, one fast and the other slow relaxing, which fully agrees with our analysis of the ZF

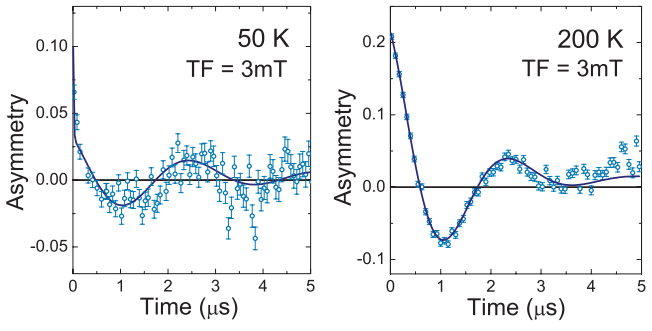

FIG. 5. (Color online) Transverse field measurement at 200 K (open symbols left) and 50 K (open symbols right). Solid line is the least-squares fit to Eq. (7).

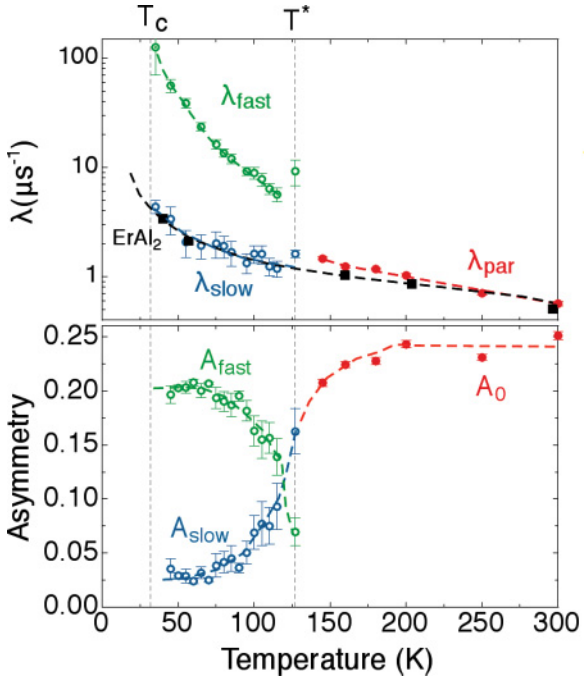

FIG. 6. (Color online) Temperature dependence of μSR parameters resulting from the fits (see text). Upper panel: the relaxation rates, in full dots the single relaxing velocity (λ_{par}), in open circles the fast (λ_{fast}) and slow relaxing rates (λ_{slow}). In full squares temperature dependence of the TF muon spin depolarization relaxation rate in $ErAl_2$ (Ref. 42). Lower panel: in full dots the temperature dependence of paramagnetic asymmetry A_0, in open circles the fast (A_{fast}) and (A_{slow}) slow asymmetries.

spectra. Similarly to Eq. (4) the value of the phase in this case is $\phi = 0$.

Figure 6 shows the temperature dependence of the μSR parameters λ_{slow}, λ_{fast}, A_0, A_{slow}, A_{fast} in the temperature regime of interest in this work ($T > T_c$). Clearly, two different regimes above T_c can be distinguished: (i) a pure paramagnetic regime above a characteristic temperature T^* (127 K) and (ii) an intermediate regime above T_c ($T_c < T < T^*$) where two very different spin relaxation rates are observed: On the one hand, λ_{slow}, which increases from ≈ 2 μs^{-1} at T^* up to ≈ 5 μs^{-1} at T_c. On the other hand, λ_{fast}, which achieves ≈ 130 μs^{-1} close to T_c, which is two orders of magnitude higher than the corresponding value of λ_{slow} at the same temperature. The strong quantitative differences between the relaxation rates below 127 K indicate the presence of a new source for muon depolarization different from pure paramagnetism. Such a remarkable difference rules out the origin of these two decays being due to slight inhomogeneities, such as a compositional distribution within the polycrystalline ingot, temperature gradients among sample grains, or any other small variations. Moreover, the slowly relaxing signal practically follows the trend of the pure paramagnetic signal, characterized by λ_{par}, observed above 127 K. This fact clearly suggests that the relaxation process at the origin of the fast-relaxing signal becomes relevant only below 127 K and coexists with a continuous source of relaxation observed from T_c to the highest studied temperatures.

It is plausible to identify the slow relaxation rate which decreases in magnitude with increasing temperature as originated by the paramagnetism in $ErCo_2$. Indeed, we may quantitatively compare both the magnitude and the temperature dependence of λ_{slow} with the paramagnetic relaxation rate measured on a simpler reference system, $ErAl_2$.[42] The latter is a ferromagnet below $T_c = 14$ K.[42,43] Above the critical temperature it is a practically ideal paramagnet[43–45] with only Er localized moments as a source of magnetism. The temperature dependence of the characteristic μSR parameter λ_{par} of $ErAl_2$ reported by Hartmann[42] is shown in the upper panel of Fig. 6. The monotonic decrease in λ_{par} with increasing temperature observed in $ErAl_2$ concurs with the variation of λ_{slow} with temperature for $T_c < T^*$. This fact allows us to identify λ_{slow} as representative of dynamic fluctuations of Er ions in the paramagnetic state. The contribution of paramagnetic Co moments ($\sim 0.2\ \mu_B$) could not be expected to be very strong, being about 40 times smaller than Er ones. In fact, above 127 K, where $ErCo_2$ appears to be properly paramagnetic, the signals from $ErCo_2$ and $ErAl_2$ coincide within the experimental error.

Therefore, it is evident that the dynamic relaxation process described by λ_{fast} below T^* in $ErCo_2$ is not originated by the fluctuation of Er ions. In general, a fast-relaxing decay indicates the development of strong spin-spin correlations. Stronger magnetic correlations between the spins slow down the spin fluctuations which leads to a remarkable rise in the relaxation rate.[28,36] Thus, our μSR results indicate the formation of short-range-order correlations below T^*. These dynamic magnetic clusters are responsible for a muon spin relaxation rate (λ_{fast}) which is about two orders of magnitude higher than the decay due to the paramagnetic fluctuations in $ErCo_2$. Taking into account previous magnetic susceptibility studies in this system, those clusters would consist of Co moments only which are ferromagnetically coupled with a size of $\approx$8 Å as characterized by SANS.[22]

The fit of the muon decay signals also yields the temperature dependence of the asymmetries A_0, A_{slow}, and A_{fast}. The lower panel of Fig. 6 shows that the signal from Co magnetic clusters (A_{fast}) increases as temperature approaches T_c, whereas A_{slow} decreases with temperature. According to the scenario described above, below T^* all the spins are still fluctuating although small dynamic clusters consisting of Co moments form small "islands" in the paramagnetic regime. As temperature decreases, the number of Co moments involved in the dynamic clustered phase increases, giving rise to both the increasing in the relaxation rate (λ_{fast}) and the corresponding signal A_{fast}, which is expected in the stabilization of a Griffiths-like state. Figure 6 shows that Co clusters formation are a more effective source of muon spin relaxation as the temperature is decreased, in agreement with the thermal evolution of the SANS and XMCD signals.

It is interesting to compare the characteristic temperatures resulting from the different experimental studies carried out so far on the paramagnetic regime of the $ErCo_2$ system, namely μSR, SANS, χ_{ac}, and XMCD. According to the present work, the cluster formation temperature occurs at $T^* \sim 127$ K. Our previous SANS experiments[22] determine the high-temperature limit for the presence of magnetic clusters at higher temperature $T^*_{SANS} = 160$ K. We ascribe such a discrepancy to the different temporal window of the μSR and SANS techniques: 1 GHz $< \nu <$ 100 THz in the SANS experiment and 100 kHz $< \nu <$ 1 GHz for the μSR measurements. Moreover, we should point out that μSR experiments are carried out at true zero applied magnetic field, whereas SANS were performed with a bias magnetic field. On the other hand, the characteristic feature in ac susceptibility measured in zero field at our highest excitation frequency available of 1 kHz appears at a frequency-dependent temperature, $T^*_{\chi_{ac}} \sim 84$ K at 1 Hz (lower than T^*). Such a characteristic temperature ($T^*_{\chi_{ac}}$) describes the relaxation process of the dynamic magnetic clusters,[26] which are formed at higher temperature (T^*). On the other hand μSR provides direct information about the formation of such dynamic clusters. Furthermore, the flipping temperature T_f determined by XMCD is the temperature at which the net cobalt moment is zero under an applied field, defining the appearance of parimagnetism. This temperature describes a different process within the paramagnetic regime which requires the clusters to have a Co negative magnetic moment overcoming the positive component of the paramagnetic fraction of Co atoms. The present μSR results indicate the formation of Co short-range correlations within the paramagnetic regime even at true zero applied field. Such a dynamic clustered phase acts as a precursor of the parimagnetism in $ErCo_2$ giving rise to the rich phenomenology reported on this system.

If a textbook paramagnet is an ideal gas of noninteracting magnetic moments, it appears clearly that $ErCo_2$ is a very strongly correlated paramagnet, in which Co has a very strong tendency to form clusters, or "droplets," suggesting a liquid-like magnetic state, rather than an ideal gas. This tendency is however reminiscent of the fact that amorphous $ErCo_2$ is a ferrimagnet due to the Co-Co interaction at temperatures as high as 470 K,[46–48] one order of magnitude higher than the T_c of crystalline $ErCo_2$.

IV. CONCLUSIONS

Muon spin relaxation spectroscopy measurements were conducted on $ErCo_2$ in order to examine the nature of the parimagnetic state recently reported on this system. Specifically, the mechanism which leads the system to transition from the disordered to the ferrimagnetic phase has been investigated. The measurements reveal the presence of an unusual paramagnetic state characterized by the development of strong spin correlations above T_c and below a characteristic temperature T^*. Analysis indicates that within this temperature range, $ErCo_2$ exhibits two independent dynamical processes: one resulting from fluctuations of Er ions (slow-relaxing signal) and another ascribed to Co clusters (fast-relaxing signal). The origin of these processes has been discussed in terms of the Co-Co short-range correlations—previously characterized by χ_{ac} and SANS—which exist within the paramagnetic state. Considering that a key feature for the formation of these short-range correlations is the ferrimagnetic nature of $ErCo_2$, the existence of parimagnetism may not be limited to this particular system. Indeed, similar behavior should be expected in other ferrimagnetic Laves phases, or in ferrimagnets within which the magnetic moments involved are of significantly different magnitudes.

ACKNOWLEDGMENTS

Financial support from the MAT08-01077 and Aragonese IMANA projects as well as from European FEDER funds is acknowledged. The authors are thankful to G. M. Kalvius for fruitful discussions and to Scott H. Williams for critical reading. C.M.B. acknowledges a Spanish MICINN grant. The authors acknowledged the Swiss muon source, SμS, at PSI.

*mbonilla@unizar.es

[1] E. P. Wohlfarth, J. Magn. Magn. Mater. **20**, 77 (1980).
[2] P. M. S. Khmelevskyi, J. Phys. Condens. Matter **12**, 9453 (2000).
[3] E. Gratz and A. S. Markosyan, J. Phys. Condens. Matter **13**, R385 (2001).
[4] J. Herrero-Albillos, F. Bartolomé, L. M. García, F. Casanova, A. Labarta, and X. Batlle, Phys. Rev. B **73**, 134410 (2006).
[5] N. H. Duc, P. E. Brommer, and K. H. J. Buschow, *Handbook on Magnetic Materials*, Vol. 12 (Elsevier, Amsterdam, 1999), p. 259.
[6] N. H. Duc, D. T. K. Anh, and P. E. Brommer, Physica B **319**, 1 (2002).
[7] A. Giguere, M. Foldeaki, W. Schnelle, and E. Gmelin., J. Phys. Condens. Matter **11**, 6969 (1999).
[8] N. A. de Oliveira, P. J. von Ranke, M. V. Tovar Costa, and A. Troper, Phys. Rev. B **66**, 094402 (2002).
[9] N. K. Singh, K. G. Suresh, A. K. Nigam, S. K. Malik, A. A. Coelho, and S. Gama, J. Magn. Magn. Mater. **317**, 68 (2007).
[10] N. H. Duc and D. T. K. Anh, J. Magn. Magn. Mater. **242-245**, 873 (2002).
[11] W. Dunhui, T. Shaolong, H. Songling, S. Zhenghua, H. Zhida, and D. Youwei, J. Alloys Compd. **360**, 11 (2003).
[12] J. Herrero-Albillos, F. Bartolomé, L. M. García, F. Casanova, A. Labarta, and X. Batlle, Phys. Rev. B **75**, 187402 (2007).
[13] C. M. Bonilla, J. Herrero-Albillos, F. Bartolomé, L. M. García, M. Parra-Borderías, and V. Franco, Phys. Rev. B **81**, 224424 (2010).
[14] A. Pirogov, A. Podlesnyak, T. Strässle, A. Mirmelstein, A. Teplykh, D. Morozov, and A. Yermakov, Appl. Phys. A **74**, s598 (2002).
[15] W. Jaeyoung, J. Younghun, H. C. Kim, A. Pirogov, J.-G. Park, H. C. Ri, A. Podlesnyak, J. Schefer, T. Strässle, and A. Teplykh, Physica B **329-333**, 653 (2003).
[16] D. Bloch, F. Chaisee, F. Givord, J. Voiron, and E. Burzo, J. Phys. **32**, C1 (1971).
[17] R. Moon, W. C. Koehler, and J. Farrell, J. Appl. Phys. **36**, 978 (1965).
[18] J. Herrero-Albillos, L. M. García, F. Bartolomé, A. Young, and T. Funk., J. Magn. Magn. Mater. **316**, e442 (2007).
[19] E. Burzo, Phys. Rev. B **6**, 2882 (1972).
[20] D. Gignoux, D. Givord, F. Givord, W. C. Koehler, and R. M. Moon, Phys. Rev. B **14**, 162 (1976).
[21] X. B. Liu and Z. Altounian, J. Phys. Condens. Matter **18**, 5503 (2006).
[22] J. Herrero-Albillos, F. Bartolomé, L. M. García, A. T. Young, T. Funk, J. Campo, and G. J. Cuello, Phys. Rev. B **76**, 094409 (2007).
[23] D. Bloch and R. Lemaire, Phys. Rev. B **2**, 2648 (1970).
[24] N. H. Duc and D. Givord, J. Magn. Magn. Mater. **151**, L13 (1995).
[25] Y. Öner, E. Alveroglu, and O. Kamer, J. Alloys Compd. **424**, 60 (2006).
[26] J. Herrero-Albillos, L. M. García, and F. Bartolomé, J. Phys. Condens. Matter **21**, 216004 (2009).
[27] J. Herrero-Albillos, L. M. García, F. Bartolomé, and A. T. Young, Europhys. Lett. **93**, 17006 (2011).
[28] G. M. Kalvius, D. R. Noakes, and O. Hartman, *Handbook on the Physics and Chemistry of Rare Earths*, Vol. 32, edited by K. A. Gschneidner *et al*. (North-Holland, Amsterdam, 2001), p. 55.
[29] N. Marcano, G. M. Kalvius, D. R. Noakes, J. C. G. Sal, R. Wäppling, J. I. Espeso, E. Schreier, A. Kratzer, C. Baines, and A. Amato, Phys. Scr. **68**, 298 (2003).
[30] R. Feyerherm, A. Amato, C. Geibel, F. N. Gygax, P. Hellmann, R. H. Heffner, D. E. MacLaughlin, R. Müller-Reisener, G. J. Nieuwenhuys, A. Schenk, and F. Steglich, Phys. Rev. B **56**, 699 (1997).
[31] A. Yaouanc and P. Dalmas de Reotier, *Muon Spin Rotation, Relaxation, and Resonance: Applications to Condensed Matter*, International Series of Monographs on Physics 147 (Oxford University Press, Oxford, 2011), p. 504.
[32] O. Hartmann, Hyperfine Interact. **49**, 61 (1989).
[33] A. Schenck, *Muon Spin Rotation Spectroscopy* (Adam Hilger, Bristol, 1985).
[34] G. M. Kalvius, A. Krimmel, O. Hartmann, F. J. Litterst, R. Wappling, V. Tsurkan, and A. Loidl, J. Phys. Condens. Matter **22**, 052205 (2010).
[35] C. Leavey, B. Rainford, and A. Hillier, Physica B: Condensed Matter **374-375**, 106 (2006).
[36] G. M. Kalvius, A. Krimmel, O. Hartmann, F. J. Litterst, R. Wappling, V. Tsurkan, and A. Loidl, Physica B: Condensed Matter **404**, 660 (2009).
[37] R. H. Heffner, J. E. Sonier, D. E. MacLaughlin, G. J. Nieuwenhuys, G. Ehlers, F. Mezei, S.-W. Cheong, J. S. Gardner, and H. Röder, Phys. Rev. Lett. **85**, 3285 (2000).
[38] Y. Öner and O. Kamer, J. Alloys Compd. **464**, 51 (2008).
[39] Y. Öner and M. Guillot, J. Appl. Phys. **105**, 07E120 (2009).
[40] A. Schenck and F. N. Gygax, *Handbook of Magnetic Materials*, Vol. 9, edited by K. H. J. Buschow (North-Holland, Amsterdam, 1995), p. 57.
[41] G. M. Kalvius, A. Krimmel, O. Hartmann, F. J. Litterst, R. Wappling, V. Tsurkan, and A. Loidl, Eur. Phys. J. B **77**, 87 (2010).
[42] O. Hartmann, E. Karlsson, R. Wäppling, J. Chappert, A. Yaouanc, L. Asch, and G. M. Kalvius, J. Phys. F **16**, 1593 (1986).
[43] H. G. Purwins and A. Leson, Adv. Phys. **39**, 309 (1990).
[44] W. Wiedemann and W. Zinn, Phys. Lett. A **24**, 506 (1967).
[45] A. L. Lima, J. Magn. Magn. Mater. **310**, 51 (2007).
[46] B. Boucher, A. Lienard, J. P. Rebouillat, and J. Schweizer, J. Phys. F **9**, 1421 (1979).
[47] B. Boucher, A. Lienard, J. P. Rebouillat, and J. Schweizer, J. Phys. F **9**, 1433 (1979).
[48] M. L. Soltani, J. Alloys Compd. **374**, 154 (2004).